Volatile Organic Compound Detection Using Insect Odorant-Receptor Functionalised Field-Effect Transistors

by

Eddyn Oswald Perkins Treacher

A thesis submitted in fulfilment of the
requirements of the degree of
Doctor of Philosophy in Physics
School of Physical and Chemical Sciences
Te Herenga Waka - Victoria University of Wellington

May 2024

Table of contents

Acknowledgements

69450

Rifat, Alex - vapour sensor Erica Cassie - FET sensing setup Rob Keyzers and Jennie Ramirez-Garcia - NMR spectra Patricia Hunt - Computational chemistry

1. Carbon Nanotube and Graphene Field-Effect Transistors

1.1. Introduction

Out of a wide range of available transducer options available for the creation of compact, portable and highly-integrated biosensors, field-effect transistors are among the most promising. Field-effect transistors consist of two conductive electrodes on either side of a semiconducting channel, the 'source' and 'drain' electrodes, alongside an isolated 'gate' electrode. An applied electric field from the gate electrode capacitively controls channel resistance, giving rise to the label 'field-effect'. By adjusting gate voltage, the flow of charge carriers between source and drain can be varied over several orders of magnitude. The ability of this simple structure to obtain a large signal response from small changes in channel behaviour means field-effect transistors can be used as high-quality amplifiers for sensor applications [1], [2]. Field-effect transistors are typically unipolar transistors; channel conduction either mainly consists of electron carriers, or hole carriers, depending on the electrode and channel materials used [2].

Carbon nanotube network and graphene field-effect transistors (CNTFETs and GFETs) are both examples of a class of field-effect transistors called thin-film transistors (TFTs). These transistors are closely related to the commonly-used metal oxide semiconductor field-effect transistor (MOSFET). Unlike MOSFETs, thin-film transistors do not use the substrate as the device channel. Instead, current passes through a semiconducting film on the surface of the device. Since thin-film transistors do not require a conductive substrate, they can be fabricated using flexible and stretchable substrates, and so are significantly more versatile than MOSFETs. A wide variety of semiconducting films may be used; the films discussed here are carbon nanotube networks and graphene, which both fall under the class of carbon-based 2D nanomaterials. Commonly used substrates include silicon/silicon dioxide, quartz, glass, and the flexible substrates polyimide (PI) and polyethylene terephthalate (PET) [1], [3].

1.2. Thin-Film Field-Effect Transistors

1.2.1. Structure and Gating

The basic components of the thin-film transistor can be configured in a variety of different ways. These configurations include the back-gated field-effect transistor and the liquid-gated transistor, also known as the electrolyte-gated transistor. The relatively simple back-gated configuration, shown in Figure 1.1 (a), uses the silicon substrate as the gate. The channel is isolated from the gate with a thin silicon dioxide layer. A liquid-gated device, shown in Figure 1.1 (b), is used for sensitive liquid analyte detection. In the most common form of this configuration, a Ag/AgCl reference electrode is used as the gate. The channel is isolated from the gate by the bulk of an electrolyte solution, typically the biofriendly phosphate-buffered saline (PBS). Other aqueous salt solutions, polymers and ion-gels are also sometimes used as the electrolyte gate. The electrolyte is restricted to the channel area using a hydrophobic PDMS microchamber, referred to here as a 'PDMS well' [1], [4], [5].

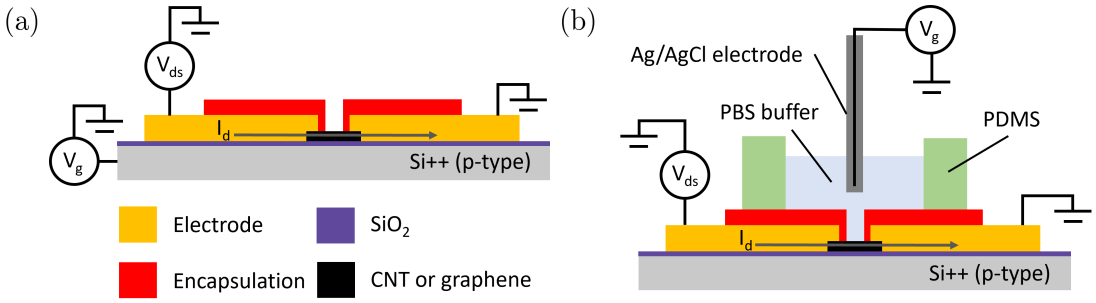

Figure 1.1.: Schematics (not to scale) showing the side-view cross-section of a thin-film field-effect transistor in both the (a) back-gated and (b) liquid-gated configuration. A graphene monolayer or a carbon nanotube network is used as the transistor thin-film. The drain electrode is the gold contact on the left side of each figure, while the source electrode is the gold contact on the right.

When the source and drain electrodes of a thin-film field-effect transistor are made of metal, a Schottky barrier forms between the channel and the electrodes. The Schottky barrier results from a difference in the work function between the metal and semiconducting channel, leading to bending of the conduction and valence bands and the formation of an electric dipole layer at the junction. Due to the absence of metal-channel bonding, the metal used has a direct impact on barrier height ϕ_B [4], [5]. The spatial extent of the dipole layer is called the barrier thickness. For unipolar transistors, where the Schottky barrier is thick, the channel-electrode contact determines the type of charge carrier passing between source and drain. A contact which forms a low Schottky barrier for holes will form a high Schottky barrier for electrons. In this case, holes flow and the device is *p*-type. The reverse applies for a contact with a high Schottky barrier for holes, where electrons flow and the device is *n*-type. Thin-film devices can also be ambipolar,

where charge carriers can quantum-mechanically tunnel through thin Schottky barriers and electrons and holes can both flow through the channel [1], [2], [4], [6].

Two different voltages are used to adjust transistor operation. The first is the 'drain bias', V_{ds}, between the drain and source electrodes, and the second is the 'gate bias', V_g, applied between the gate and source electrode. Changing V_g alters the energy band bending at the channel-electrode junctions, and therefore also alters the energy barriers at these junctions. The value of V_g therefore determines whether charge carriers may flow under the influence of V_{ds} and produce a drain-source current I_d; in other words, V_g determines whether the transistor is 'on' or 'off'. The threshold voltage V_t is the gate voltage required to increase the Schottky barrier height to a point where charge carriers no longer flow. For a *p*-type semiconductor channel, increasing V_g towards positive gate voltages will raise the Schottky barrier and turn current off, with the opposite being true for an *n*-type channel. In an ambipolar transistor, a highly negative V_g will give rise to hole conduction, and a highly positive V_g will give rise to electron conduction. There are therefore two threshold voltages for these devices, $V_{t,h}$ and $V_{t,e}$. Within the range between these gate voltages, both holes and electrons flow through the channel [2], [4], [5], [7].

The type of structure used determines the type of biological sensing mechanisms available, which can include electrostatic gating, Schottky barrier modulation, capacitance modulation or charge scattering. Response mechanisms may take place at the gate, at the junctions between channel and contact, or within the semiconductor channel [5], [6]. The encapsulation layer shown in Figure 1.1 is added to separate the electrodes from the channel-metal junction, ensuring that the less-reliable response due to modification of the channel-metal Schottky barrier does not dominate sensing [2], [6]. Encapsulation is therefore a vital part of a functioning sensor, despite being under-examined in the literature [1]. In an encapsulated device with a semiconducting thin-film, the predominant sensing mechanism is electrostatic gating. Here, the presence of a positive charge induces negative charge in the channel or *vice versa*, in effect doping the channel and altering the relationship between V_g and I_d [6]. The relative effect of changes in V_g on I_d is determined by gate capacitance, which is a series combination of the geometric capacitance, C_G, and the quantum capacitance of the 2D nanomaterial, C_Q. For a back-gated device, geometric capacitance is predominantly due to the oxide layer capacitance C_{ox} [5], [8].

Liquid-Gating and Debye Length

Understanding the ionic behaviour of the gate electrolyte used in a liquid-gated device setup gives insight into the gating and sensing behaviour of the setup. When a voltage is applied at the liquid-gate, the charged ions in solution move to form two electric double layers, one at the interface between the electrolyte and gate electrode, and one at the interface between electrolyte and semiconducting channel, as shown in Figure 1.2. The gate capacitance is a series combination of the capacitance of each EDL in series

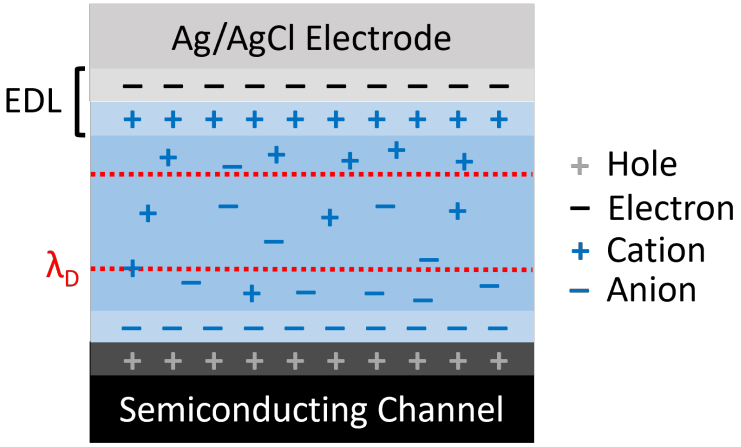

Figure 1.2.: A diagram of the formation of an electric double layer (EDL) under an applied voltage between source and liquid-gate electrodes, with a p-type semiconductor used for the channel thin-film. Electric double layers are present at both the gate-electrolyte interface and semiconductor-electrolyte interface. Adapted from [1], [9]

with quantum capacitance C_Q. The Gouy-Chapman-Stern model splits the EDL into two distinct regions, the first being a compact layer of ions, the Stern layer, and the second being a more diffuse layer, the Gouy-Chapman layer. The surface potential of the solid-electrolyte interface exponentially decreases across the diffuse region of the double-layer; the characteristic length of this potential screening is known as Debye length, λ_D. The typical electrolyte Debye length is on a nanometer scale, therefore the bulk electrolyte acts as an insulator, similar to the silicon dioxide dielectric in the back-gated configuration. The Stern layer capacitance is inversely proportional to the Debye length, and therefore decreased λ_D corresponds to increased gate capacitance [1], [9]–[11].

$$\lambda_D = \sqrt{\frac{\epsilon_0 \epsilon_r k_b T}{2 N_A q^2 I}} \tag{1.1}$$

The equation for Debye length λ_D in an electrolyte solution is given by Equation 1.1, where ϵ_0 is vacuum permittivity, ϵ_r is the relative permittivity of the electrolyte, B is the Boltzmann constant, T is absolute temperature in K, N_A is the Avogadro number, q is the elementary charge and I is ionic strength in mmol L^{-1}. When temperature is kept constant, λ_D only depends on the ionic strength of the electrolyte and not on any attributes of the gate electrode or channel. Successive dilutions of a particular electrolyte will increase the Debye length: for 1× PBS, λ_D is 0.7 nm, for 0.1× PBS, λ_D is 2.3 nm, for 0.01× PBS λ_D is 7.3 nm and so on. This means gate capacitance is directly dependent on the electrolyte used and its concentration. A 1× PBS electrolyte gives a

gate capacitance several orders of magnitude larger than that of a silicon oxide back-gate, where a larger capacitance significantly increases the effect of electrostatic gating on the channel current. A liquid-gated device with low Debye length will therefore be highly sensitive to electrostatic changes across a small voltage range [1], [11].

However, a decreased Debye length also has disadvantages for sensing. Electrostatic potentials outside of the electrolyte-channel electrical double layer are effectively screened from the channel. Electrical double layers will also form around biomolecules such as DNA present within the solution. The combined screening effect means signals due to potential changes in charged biomolecules within the bulk electrolyte will have no effect on gating of the channel. Interactions between the analyte and any biorecognition element must therefore occur within the Debye length. A tradeoff has to be made between channel sensitivity and the size of the sensitive region above the channel. Many medium or large proteins will require a relatively dilute electrolyte for analyte capture to be detected by the channel [1], [12], [13]. Other approaches to increasing Debye length without reducing device sensitivity have also been trialled. One approach is to attach a layer of polyethylene glycol polymer (PEG) to the device, reducing the ability of counterions to approach the channel. This increases Debye length at the electrolyte-channel interface while preserving the capacitance of the electrolyte-gate interface, keeping device sensitivity relatively high [14], [15].

1.2.2. Electrical Characterisation

Both carbon nanotube field effect transistors and graphene field-effect transistors are naturally ambipolar [4], [8]. As described in Section 1.2.1, applying a gate voltage V_g to the gate of an ambipolar thin-film transistor influences the amount and type of available charge carriers through altering the channel energy bands and therefore the electrode-channel Schottky barriers. The current-voltage plots for a given transistor are known as the 'characteristic curves' of the transistor. The plot of I_d against V_g at constant V_{ds} is known as the 'transfer' characteristic curve at that source-drain voltage, while the I-V curve of I_d against V_{ds} at constant V_g is known as the 'source-drain' or 'output' characteristic curve at that gate voltage [16]. Device transfer characteristics are dictated by the gate capacitance, as discussed in Section 1.2.1. An example of both back-gated and liquid-gated transfer characteristics from ambipolar thin-film transistors are shown in Figure 1.3.

When source-drain bias voltage is small, the output characteristic curve is linear [4]. In this linear regime, transconductance at a specific gate voltage is given by $g_m = |dI_d/dV_g|$. Transconductance indicates how responsive the device is to electrostatic gating at a given gate voltage. In other words, when g_m is large, small changes in V_g can significantly modulate channel current I_d, which is useful for sensing [8]. Transconductance at a given gate voltage is also proportional to the mobility of charge carriers in the device channel [5], [17]. The transconductance at a specific gate voltage can be found from performing a linear fit in a small region around that voltage on the transfer curve. Linear fits for

transconductance at $V_g = 0$ V are shown for a back-gated device in Figure 1.3 (a), and a liquid-gated device in Figure 1.3 (b), which give values of $g_m = 5 \times 10^{-8} S$ and $g_m = 100 \times 10^{-8} S$ respectively. Note the order of magnitude difference between back-gated transconductance and liquid-gated transconductance. Applying the gate voltage that gives maximum transconductance may not always be the optimal sensing setup, however. Heller *et al.* argued that gating carbon nanotube devices in the subthreshold regime led to sensing with superior signal-to-noise ratio [18].

For the liquid-gated case, the choice of electrolyte determines the appropriate voltage range for electrical characterisation, as excessive voltages will induce redox reactions. For water-based electrolytes, gate voltages must be kept within the $±$1 V range [1].

An important attribute of the transfer characteristic curve for all thin-film FETs is the on-off current ratio. On-off current ratio is the ratio of the current through a device when gated fully 'off' with a positive voltage, to the current through the device when gated fully 'on' with a negative voltage [17]. The off current in an ambipolar FET can be defined as the minimum current during the transfer sweep, where the majority carrier transitions from being holes to electrons or vice versa. For example, the on current of the channel shown in Figure 1.3 (b) is 741.5 nA, the off current is 0.2 nA, and therefore the on-off ratio is ~ 3000. In contrast, even when 10 V is applied, the backgated device shown in Figure 1.3 (a) is never gated fully off. Application of higher voltages to the gate result in significant leakage currents through the gate, and can even result in irreversible breakdown of the oxide layer [16]. Being able to traverse both on and off regimes over a limited voltage interval is one of the many advantages of the liquid-gated configuration.

V_t can be estimated by extrapolating the linear region of the transfer characteristics of a device to the V_g axis. The value for V_g at this intercept is approximately equal to V_t when V_{ds} is close to zero [16]. It should be noted that it is difficult to relate this estimate for V_t for thin-film field-effect transistors to carrier density directly. Instead, the value found for V_t should be considered as a useful parameter for comparing the gating behaviour of different devices [**Schoonveld2001**].

subthreshold regime Previous biosensor research

As $C_{qm} \gg C_{edl}$, hysteresis is significantly reduced for the liquid-gated configuration relative to the back-gated configuration. In this work, the liquid-gate is completely isolated from the channel, which ensures sensing is not due to modulation of the Schottky barrier between the channel and electrodes, but this is not always true for thin-film transistors in the literature [5].

Channel carriers in a FET can be accelerated by a sufficiently high gate-channel field into surmounting the insulating barrier between the gate and channel. This is known as 'breakdown'. The breakdown voltage V_b gives an upper limit to the bias able to be applied across the device without the device being destroyed. Percolation theory can be used to explain breakdown. As energetic carriers pass through the oxide, defects are created randomly. When these random defects are dense enough to form a chain from the gate to the semiconductor, a short is created and breakdown occurs. With decreased

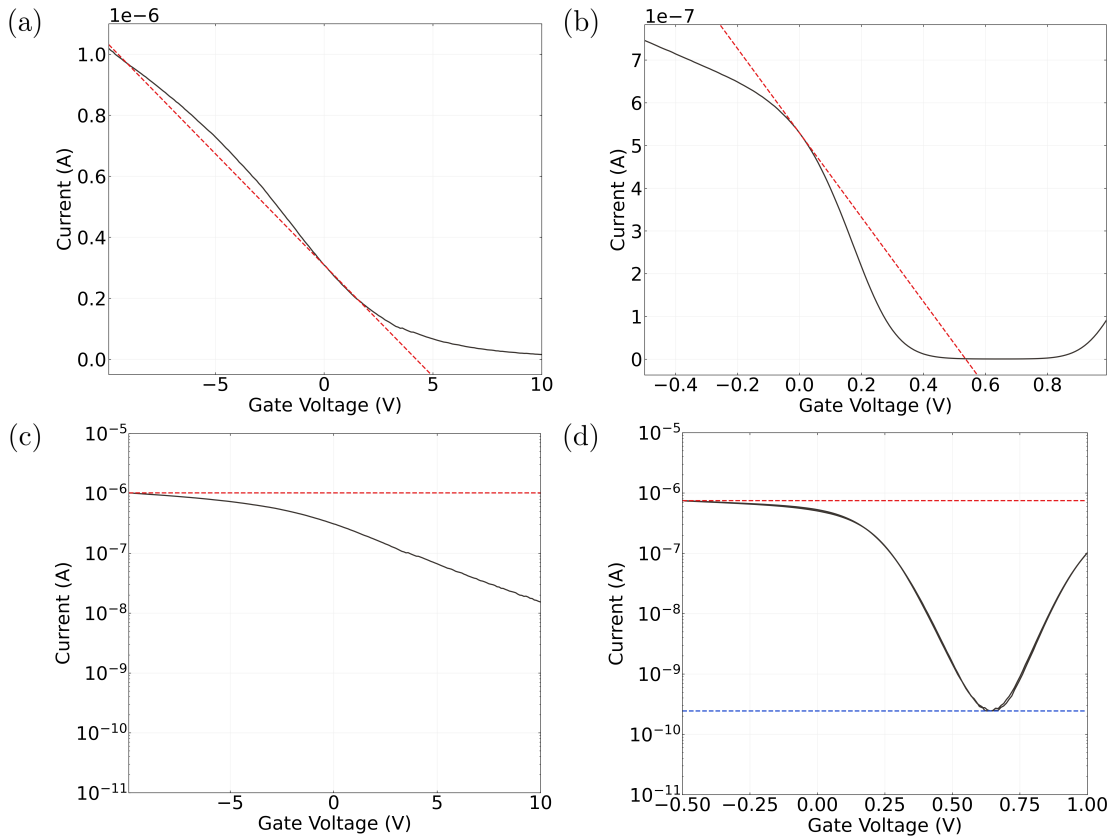

Figure 1.3.: Examples of field-effect transistor transfer characteristics taken at $V_{ds} = 100$ mV from two different device channels. A linear scale is used in (a) and (b), while a logarithmic scale is used in (c) and (d). The device channel in (a) and (c) was backgated while the device channel in (b) and (d) was liquid-gated. The linear fit with gradient corresponding to transconductance at $V_g = 0$ V is shown in (a) and (b) with a dotted red line. The "on" current in (c) and (d) is shown with a red horizontal line, while the "off" current in (d) is shown with a blue horizontal line.

oxide thickness the the required voltage for breakdown also decreases, due to increased carrier tunnelling.

- oxide layer leakages

Then leakage also occurs when electrolyte conducts

1.2.3. Current Sampling

It is important to account for the changes in current that occur during a sensing run that are unrelated to sensing, and try to minimise these changes as much as possible. These changes are due to a variety of causes and can be categorised as various types of noise and baseline drift. (1/f noise paper, heller paper)

1.3. Graphene Field-Effect Transistors

1.3.1. Electrical Characterisation

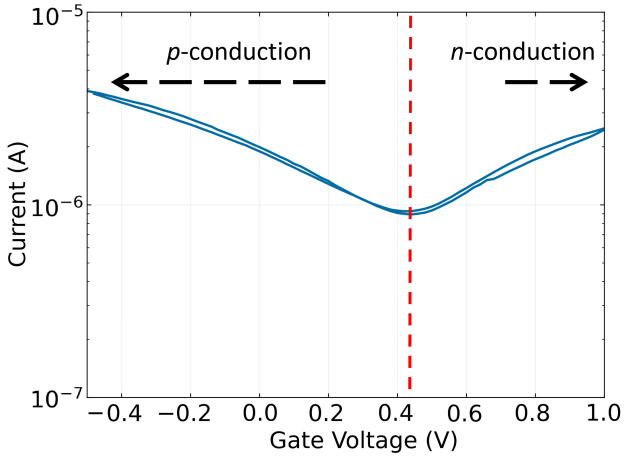

Figure 1.4.: Transfer characteristics of a graphene field-effect transistor channel showing the regions of hole conduction and electron conduction. The red dotted line indicates the Dirac point voltage of the device channel.

As graphene field-effect transistors do not possess a characteristic 'off' regime. In normal operation of a GFET, the lowest voltage obtainable by gating is known as the Dirac voltage [19].

Quantative measurement of leftward shift in transfer curve Use minima of curve in reverse sweep direction (more consistent than reading in forward sweep direction) I compared the

transfer characteristics after then rinse steps to the pristine characteristics Transfer shifts where current drops to zero are excluded (indicates delamination/damage to channel)

1.4. Random-Network Carbon Nanotube Field-Effect Transistors

1.4.1. Composition and Chirality

A single-walled carbon nanotube (SWCNT) consists of a graphene sheet, a flat carbon lattice with hexagonal cells, rolled up into a cylinder. Since their discovery in 1991, a wide range of device applications for carbon nanotubes (CNTs) have been proposed, based on CNTs being highly sensitive to their environment [20], [21]. This high sensitivity is due to the high surface-to-volume ratio of the CNTs, which maximises the exposure of this electrically sensitive structure to its surroundings [1], [2]. SWCNT-based devices consume little power, operate quickly and are highly flexible [1]. Nanotubes in a network can have semiconducting characteristics (s-CNTs) or metallic characteristics (m-CNTs), depending on their chirality [22], [23]. A single CNT will therefore have different properties than a network of CNTs, where the individual electrical properties of the CNT tubes are averaged out across the network [24]. The contact between the electrodes and carbon nanotubes determines the behaviour of channel carriers. The properties of electrodes generally used in CNT FETs means they usually operate as p-type transistors [2].

Able to conduct ballistically, good coupling between gate and channel electric fields with carbon nanotube devices which enables shorter channel sizes [4] carbon nanotube devices in the electrolyte-gated layout have stronger channel-gate coupling than the back-gated layout [8]

Semiconducting carbon nanotubes have particular advantages for use in sensor applications, including a high carrier mobility, compatibility with many biological targets, and ease of processing [1].

1.4.2. Carbon Nanotube Networks

Schottky barriers form between the metallic and semiconducting carbon nanotubes within a network

1.4.3. Electrical Characterisation

Like graphene transistors, carbon nanotube transistors are naturally ambipolar: they can conduct both electrons and holes. Holes travel at highly negative voltages, while

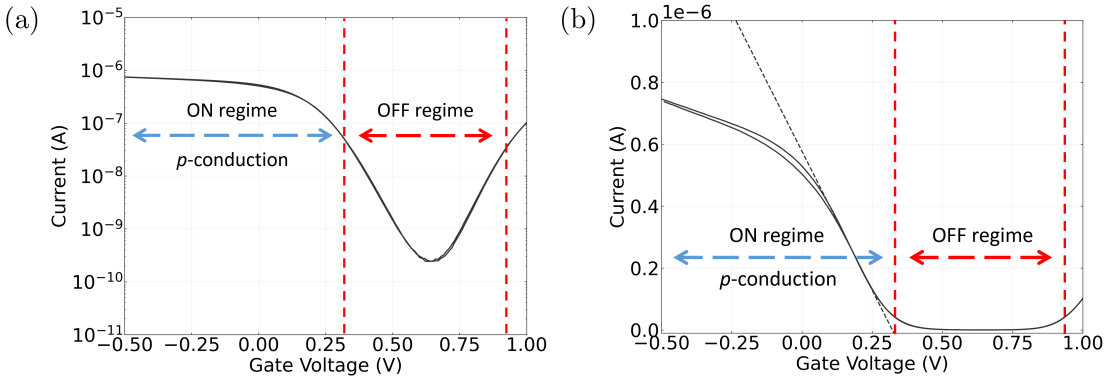

Figure 1.5.: Transfer characteristics of a single carbon nanotube network field-effect transistor channel, using a logarithmic scale in (a) and using a linear scale in (b) to emphasise different features of the same dataset. The subthreshold slope is shown with a black dotted line, while the threshold voltages are shown with red dotted lines. The ON and OFF regimes are also indicated on both figures.

electrons travel at highly positive voltages. At intermediary voltages, both electrons and holes flow. Carbon nanotube transistors can also be doped into behaving as a unipolar transistor [4]. If heavily oxygen doped, the semiconducting carbon nanotubes will exhibit p-type behaviour, with current flow only occuring in a negative bias state [1].

Threshold Voltage

The threshold voltage is the voltage required to fully deplete the device channel of charge carriers [22]. It can be estimated by extrapolating the linear part of the transfer characteristics of a device to the V_g axis.

The FET turns on at the 'threshold voltage', $V_g = V_t$. For the p-type FET, when $V_g > V_t$, I_d increases linearly.

After decreasing past V_t, I_d stays constant at its 'on' value I_{ON}. The ratio of I_{ON} to the I_{OFF} current is known as the FET device's 'on-off ratio', I_{ON}/I_{OFF}. The threshold voltage can be calculated by using an FET's transfer characteristics. From extrapolating the trendline of the linear region to the V_g axis, the intercept V_{gInt} is approximately equivalent to V_t [16].

Threshold Voltage: minimum gate-to-source voltage that is needed to create a conducting path between the electrodes

Quantative measurement of leftward shift in transfer curve Use minima of curve in reverse sweep direction (more consistent than reading in forward sweep direction) I compared the

transfer characteristics after then rinse steps to the pristine characteristics Transfer shifts where current drops to zero are excluded (indicates delamination/damage to channel)

Second quantative measurement of leftward shift in transfer curve Use curve in reverse sweep direction (more consistent than reading in forward sweep direction) Separate readings for left and right hand sides of transfer curve (left side = electrons dominant carrier, right side = holes dominant carrier) Transfer shifts where current drops to zero are excluded (indicates delamination/damage to channel) This gives us a quantitative idea of whether the transfer shifts in slides 5/6 are stable (remain the same/similar after rinse steps)

A. Vapour System Hardware

Table A.1.: Major components used in construction of the vapour delivery system described in this thesis.

Description	Part No.	Manufacturer
Mass flow controller, 20 sccm full scale	GE50A013201SBV020	MKS Instruments
Mass flow controller, 200 sccm full scale	GE50A013202SBV020	MKS Instruments
Mass flow controller, 500 sccm full scale	FC-2901V	Tylan
Analogue flowmeter, 240 sccm max. flow	116261-30	Dwyer
Micro diaphragm pump	P200-B3C5V-35000	Xavitech
Analogue flow controller, for micro diaphragm pump	X3000450	Xavitech
10 mL Schott bottle	218010802	Duran
PTFE connection cap system	Z742273	Duran
Baseline VOC-TRAQ flow cell, red	043-951	Mocon
Humidity and temperature sensor	T9602	Telaire
Enclosure, for humidity and temperature sensor	MC001189	Multicomp Pro

B. Python Code for Data Analysis

B.1. Code Repository

The code used for general analysis of field-effect transistor devices in this thesis was written with Python 3.8.8. Contributors to the code used include Erica Cassie, Erica Happe, Marissa Dierkes and Leo Browning. The code is located on GitHub and the research group OneDrive, and is available on request.

B.2. Atomic Force Microscope Histogram Analysis

The purpose of this code is to analyse atomic force microscope (AFM) images of carbon nanotube networks in .xyz format taken using an atomic force microscope and processed in Gwyddion (see **?@sec-afm-characterisation**). It was originally designed by Erica Happe in Matlab, and adapted by Marissa Dierkes and myself for use in Python. The code imports the .xyz data and sorts it into bins 0.15 nm in size for processing. To perform skew-normal distribution fits, both *scipy.optimize.curve_fit* and *scipy.stats.skewnorm* modules are used in this code.

B.3. Raman Spectroscopy Analysis

The purpose of this code is to analyse a series of Raman spectra taken at different points on a single film (see **?@sec-raman-characterisation**). Data is imported in a series of tab-delimited text files, with the low wavenumber spectrum ($100\ \mathrm{cm}^{-1} - 650\ \mathrm{cm}^{-1}$) and high wavenumber spectrum ($1300\ \mathrm{cm}^{-1} - 1650\ \mathrm{cm}^{-1}$) imported in separate datafiles for each scan location.

B.4. Field-Effect Transistor Analysis

The purpose of this code is to analyse electrical measurements taken of field-effect transistor (FET) devices. Electrical measurements were either taken from the Keysight 4156C Semiconductor Parameter Analyser, National Instruments NI-PXIe or Keysight B1500A Semiconductor Device Analyser as discussed in **?@sec-electrical-characterisation**;

the code is able to analyse data in .csv format taken from all three measurement setups. The main Python file in the code base consists of three related but independent modules: the first analyses and plots sensing data from the FET devices, the second analyses and plots transfer characteristics from channels across a device, and the third compares individual channel characteristics before and after a modification or after each of several modifications. The code base also features a separate config file and style sheet which govern the behaviour of the main code. The code base was designed collaboratively by myself and Erica Cassie over GitHub using the Sourcetree Git GUI.

Bibliography

[1] Bajramshahe Shkodra, Mattia Petrelli, Martina Aurora Costa Angeli, et al. "Electrolyte-gated carbon nanotube field-effect transistor-based biosensors: Principles and applications". In: *Applied Physics Reviews* 8.4 (Dec. 2021), p. 41325. ISSN: 19319401. DOI: 10.1063/5.0058591/1076095. URL: /aip/apr/article/8/4/041325/1076095/Electrolyte-gated-carbon-nanotube-field-effect.

[2] Xuesong Yao, Yalei Zhang, Wanlin Jin, et al. "Carbon Nanotube Field-Effect Transistor-Based Chemical and Biological Sensors". In: *Sensors 2021, Vol. 21, Page 995* 21.3 (Feb. 2021), p. 995. ISSN: 1424-8220. DOI: 10.3390/S21030995. URL: https://www.mdpi.com/1424-8220/21/3/995/htm%20https://www.mdpi.com/1424-8220/21/3/995.

[3] Dong Ming Sun, Chang Liu, Wen Cai Ren, et al. "A Review of Carbon Nanotube- and Graphene-Based Flexible Thin-Film Transistors". In: *Small* 9.8 (Apr. 2013), pp. 1188–1205. ISSN: 1613-6829. DOI: 10.1002/SMLL.201203154. URL: https://onlinelibrary.wiley.com/doi/full/10.1002/smll.201203154%20https://onlinelibrary.wiley.com/doi/abs/10.1002/smll.201203154%20https://onlinelibrary.wiley.com/doi/10.1002/smll.201203154.

[4] Phaedon Avouris. "Electronics with carbon nanotubes". In: *Physics World* 20.3 (Mar. 2007), p. 40. ISSN: 2058-7058. DOI: 10.1088/2058-7058/20/3/32. URL: https://iopscience.iop.org/article/10.1088/2058-7058/20/3/32%20https://iopscience.iop.org/article/10.1088/2058-7058/20/3/32/meta.

[5] Zhongyu Li, Mengmeng Xiao, Chuanhong Jin, et al. "Toward the Commercialization of Carbon Nanotube Field Effect Transistor Biosensors". In: *Biosensors 2023, Vol. 13, Page 326* 13.3 (Feb. 2023), p. 326. ISSN: 2079-6374. DOI: 10.3390/BIOS13030326. URL: https://www.mdpi.com/2079-6374/13/3/326/htm%20https://www.mdpi.com/2079-6374/13/3/326.

[6] Iddo Heller, Anne M. Janssens, Jaan Männik, et al. "Identifying the mechanism of biosensing with carbon nanotube transistors". In: *Nano Letters* 8.2 (Feb. 2008), pp. 591–595. ISSN: 15306984. DOI: 10.1021/NL072996I. URL: https://pubs.acs.org/doi/full/10.1021/nl072996i.

[7] Ciril Reiner-Rozman, Melanie Larisika, Christoph Nowak, et al. "Graphene-Based Liquid-Gated Field Effect Transistor for Biosensing: Theory and Experiments". In: *Biosensors & bioelectronics* 70 (Aug. 2015), p. 21. ISSN: 18734235. DOI: 10.1016/J.BIOS.2015.03.013. URL: /pmc/articles/PMC4707551/%20/pmc/articles/PMC4707551/?report=abstract%20https://www.ncbi.nlm.nih.gov/pmc/articles/PMC4707551/.

[8] I. Heller, S. Chatoor, J. Männik, et al. "Comparing the weak and strong gate-coupling regimes for nanotube and graphene transistors". In: *physica status solidi (RRL) – Rapid Research Letters* 3.6 (Sept. 2009), pp. 190–192. ISSN: 1862-6270. DOI: 10.1002/PSSR.200903157. URL: https://onlinelibrary.wiley.com/doi/full/10.1002/pssr.200903157%20https://onlinelibrary.wiley.com/doi/abs/10.1002/pssr.200903157%20https://onlinelibrary.wiley.com/doi/10.1002/pssr.200903157.

[9] Pranjala Tiwari and Dawid Janas. "Emergent pseudocapacitive behavior of single-walled carbon nanotube hybrids: a materials perspective". In: *Materials Chemistry Frontiers* 6.17 (Aug. 2022), pp. 2386–2412. ISSN: 20521537. DOI: 10.1039/D2QM00146B. URL: https://pubs.rsc.org/en/content/articlehtml/2022/qm/d2qm00146b%20https://pubs.rsc.org/en/content/articlelanding/2022/qm/d2qm00146b.

[10] Allen J. Bard and Larry R. Faulkner. "Double-layer structure and adsorption". In: *Electrochemical methods : fundamentals and applications*. 2nd ed. 4. New York: Wiley, 2001. Chap. 13, pp. 534–579. ISBN: 0471043729.

[11] Jacob N. Israelachvili. "Electrostatic Forces between Surfaces in Liquids". In: *Intermolecular and Surface Forces* (Jan. 2011), pp. 291–340. DOI: 10.1016/B978-0-12-375182-9.10014-4.

[12] Eric Stern, Robin Wagner, Fred J. Sigworth, et al. "Importance of the debye screening length on nanowire field effect transistor sensors". In: *Nano Letters* 7.11 (Nov. 2007), pp. 3405–3409. ISSN: 15306984. DOI: 10.1021/NL071792Z/SUPPL_FILE/NL071792ZSI20070910_015801.PDF. URL: https://pubs.acs.org/doi/full/10.1021/nl071792z.

[13] Esteban Piccinini, Sebastián Alberti, Gabriel S. Longo, et al. "Pushing the Boundaries of Interfacial Sensitivity in Graphene FET Sensors: Polyelectrolyte Multilayers Strongly Increase the Debye Screening Length". In: *Journal of Physical Chemistry C* 122.18 (May 2018), pp. 10181–10188. ISSN: 19327455. DOI: 10.1021/ACS.JPCC.7B11128/ASSET/IMAGES/MEDIUM/JP-2017-11128H_M007.GIF. URL: https://pubs.acs.org/doi/full/10.1021/acs.jpcc.7b11128.

[14] Ning Gao, Teng Gao, Xiao Yang, et al. "Specific detection of biomolecules in physiological solutions using graphene transistor biosensors". In: *Proceedings of the National Academy of Sciences of the United States of America* 113.51 (Dec. 2016), pp. 14633–14638. ISSN: 10916490. DOI: 10.1073/PNAS.1625010114/SUPPL_FILE/PNAS.201625010SI.PDF. URL: https://www.pnas.org/doi/abs/10.1073/pnas.1625010114.

[15] Vladimir Kesler, Boris Murmann, and H. Tom Soh. "Going beyond the Debye Length: Overcoming Charge Screening Limitations in Next-Generation Bioelectronic Sensors". In: *ACS Nano* 14.12 (Dec. 2020), p. 16194. ISSN: 1936086X. DOI: 10.1021/ACSNANO.0C08622. arXiv: 2007.13201. URL: /pmc/articles/PMC7761593/%20/pmc/articles/PMC7761593/?report=abstract%20https://www.ncbi.nlm.nih.gov/pmc/articles/PMC7761593/.

[16] S.M. Sze and Kwok K. Ng. "Physics of Semiconductor Devices". In: *Physics of Semiconductor Devices* (Oct. 2006). DOI: 10.1002/0470068329. URL: https://onlinelibrary.wiley.com/doi/book/10.1002/0470068329.

[17] H. Y. Zheng and N. O.V. Plank. "Facile fabrication of carbon nanotube network thin film transistors for device platforms". In: *International Journal of Nanotechnology* 14.1-6 (2017), pp. 505–518. ISSN: 14757435. DOI: 10.1504/IJNT.2017.082473.

[18] Iddo Heller, Jaan Mãnnik, Serge G. Lemay, et al. "Optimizing the signal-to-noise ratio for biosensing with carbon nanotube transistors". In: *Nano Letters* 9.1 (Jan. 2009), pp. 377–382. ISSN: 15306984. DOI: 10.1021/NL8031636. URL: https://pubs.acs.org/doi/full/10.1021/nl8031636.

[19] Thanihaichelvan Murugathas, Cyril Hamiaux, Damon Colbert, et al. "Evaluating insect odorant receptor display formats for biosensing using graphene field effect transistors". In: *ACS Applied Electronic Materials* 2.11 (Nov. 2020), pp. 3610–3617. ISSN: 26376113. DOI: 10.1021/ACSAELM.0C00677. URL: https://pubs.acs.org/doi/full/10.1021/acsaelm.0c00677.

[20] Sumio Iijima. "Helical microtubules of graphitic carbon". In: *Nature 1991 354:6348* 354.6348 (1991), pp. 56–58. ISSN: 1476-4687. DOI: 10.1038/354056a0. URL: https://www.nature.com/articles/354056a0.

[21] Cees Dekker. "Carbon Nanotubes as Molecular Quantum Wires". In: *Physics Today* 52.5 (May 1999), pp. 22–28. ISSN: 0031-9228. DOI: 10.1063/1.882658. URL: /physicstoday/article/52/5/22/410816/Carbon-Nanotubes-as-Molecular-Quantum-WiresThe.

[22] R. Martel, T. Schmidt, H. R. Shea, et al. "Single- and multi-wall carbon nanotube field-effect transistors". In: *Applied Physics Letters* 73.17 (Oct. 1998), pp. 2447–2449. ISSN: 0003-6951. DOI: 10.1063/1.122477. URL: /aip/apl/article/73/17/2447/1023171/Single-and-multi-wall-carbon-nanotube-field-effect.

[23] Jing Kong, Nathan R. Franklin, Chongwu Zhou, et al. "Nanotube molecular wires as chemical sensors". In: *Science (New York, N.Y.)* 287.5453 (Jan. 2000), pp. 622–625. ISSN: 1095-9203. DOI: 10.1126/SCIENCE.287.5453.622. URL: https://pubmed.ncbi.nlm.nih.gov/10649989/.

[24] Yann Battie, Olivier Ducloux, Philippe Thobois, et al. "Evaluation of sorted semiconducting carbon nanotube films for gas sensing applications". In: *Comptes Rendus Physique* 11.5-6 (June 2010), pp. 397–404. ISSN: 1631-0705. DOI: 10.1016/J.CRHY.2010.06.004.